DOI: 10.1002/ejic.200700870

Synthesis, Characterization and Quantum Mechanical Calculations of $[Au_{18}Se_8(dppthph)_6]Cl_2$

Paloma Sevillano,[a] Olaf Fuhr,[a] Oliver Hampe,[a] Sergej Lebedkin,[a] Christian Neiss,[a] Reinhart Ahlrichs,[a,b] Dieter Fenske,*[a,c] and Manfred M. Kappes[a,b]

Keywords: Cluster complexes / SCS-MP2 calculations / FT-ESI mass spectrometry / Gold / Photoluminescence measurements / Selenium

The reaction of [Au(tht)Cl] (tht = tetrahydrothiophene) with 2,5-bis(diphenylphophanyl)thiophene (dppthph) and Se-$(SiMe_3)_2$ leads to the formation of $[Au_{18}Se_8(dppthph)_6]Cl_2$. This compound crystallizes in two modifications, both containing a cluster dication with nearly identical gold–selenium cores. The dication consists of two subunits only connected by six aurophilic interactions. ESI MS demonstrates that these facilitate cohesion of the cluster subunits even in the gaseous state. SCS-MP2 calculations show that the dimer is a metasable species, which is ultimately prevented from dissociation by a Coulomb barrier. In addition, photoluminescene measurements demonstrate that the small differences in the ligand shell of the cluster molecules lead to different photoluminescene properties of the two modifications.

Introduction

During the last years much attention has been paid to the rich chemistry of ligand-stabilized gold-containing clusters, which has been extensively studied.[1,2] In previous works, we have reported about different gold cluster compounds containing elements from the groups 15 and 16. While the compounds containing selenium bridges seem to favor species containing 10 or 18 gold atoms, with Au_3Se fragments as building blocks of the larger structures,[2a–2d] the clusters containing phosphorus and arsenic bridges show more versatile arrangements containing 10, 12, 17, 18 or 19 gold atoms and different building blocks like Au_4P_2, Au_4As_2 or Au_7P_2 in $[Au_{12}(PPh)_2(P_2Ph_2)_2(dppm)_4Cl_2]Cl_2$, $[Au_{17}(As\mathit{n}Pr)_6(As_2\mathit{n}Pr_2)(dppm)_6]Cl_3$ and $[Au_{18}(P)_2(PPh)_4(PHPh)(dppm)_6]Cl_3$, respectively.[2e–2g] In all these compounds, the building blocks are bridged by the diphosphane ligands with the length of their carbon chains being a determining factor affecting the final geometry of the cluster compound. In this work we report the synthesis and characterization of the compound $[Au_{18}Se_8(dppthph)_6]Cl_2$ (**1**) [dppthph = 2,5-bis(diphenylphosphanyl)thiophene].

Results and Discussion

The reaction of the gold(I) complex [Au(tht)Cl] (tht = tetrahydrothiophene), the phosphane dppthph and Se-$(SiMe_3)_2$ leads to the formation of the compound $[Au_{18}Se_8(dppthph)_6]Cl_2$ (**1**). It crystallizes in two different space groups, $P\bar{1}$ (**1a**) and $P2_12_12_1$ (**1b**), which results in crystals with different appearance and colors: yellow rectangular plates and orange highly faceted hexagonal blocks, respectively (Scheme 1).

$$[Au(tht)Cl] + dppthph + Se(SiMe_3)_2 \xrightarrow{CH_2Cl_2} [Au_{18}Se_8(dppthph)_6]Cl_2\ (\mathbf{1a}\text{ and }\mathbf{1b})$$

Scheme 1. Preparation reaction of compound **1**.

Single-crystal X-ray analysis has been carried out for **1a** and **1b**. The results are shown in Figure 1.[3] Figure 1a shows a superposition of the $[Au_{18}Se_8(dppthph)_6]^{2+}$ cations in **1a** (blue) and **1b** (orange) indicating that the Au–Se cores are nearly identical concerning bond lengths and angles. One main difference in the molecular structures of **1a** and **1b** is the different orientation of the thiophene rings of the phosphane ligands (also the orientations of the phenyl rings – not shown in Figure 1 – differ, probably due to packing effects). Figure 1b shows a labelled model of the cation in **1a**. It consists of two separate $[Au_9Se_4(dppthph)_3]^+$ subunits, each of which is formed by four corner-sharing trigonal Au_3Se pyramids (red and green polyhedra). This arrangement is typical for cluster compounds of the composition $[Au_{18}E_8(dppthph)_6]^{2+}$ (E: chalcogen; dppx: bidentate phosphane).[2a,4] All gold atoms in **1a** are almost linearly coordinated (bond angles between 167.5° and 177.2°) either by two selenium atoms or by one selenium atom and one phosphorus atom of the dppthph ligands. In the inner part of the cluster there are six relatively short Au···Au distances [294.5(1)–301.1(1) pm; indicated by dashed lines in Figure 1b] between gold atoms of different subunits (Au1–Au3

[a] Institut für Nanotechnologie, Forschungszentrum Karlsruhe, Postfach 3640, 76021 Karlsruhe, Germany
[b] Institut für Physikalische Chemie, Universität Karlsruhe, 76128 Karlsruhe, Germany
[c] Institut für Anorganische Chemie, Universität Karlsruhe, 76128 Karlsruhe, Germany
Fax: +49-721-608-8440
E-mail: dieter.fenske@aoc1.uni-karlsruhe.de

and Au10–Au12) forming an Au_6Se_2 heterocubane-like motif. A view from a different angle (Figure 1c, Au···Au not drawn) shows that there is no additional chemical bond between the two $[Au_9Se_4(dppthph)_3]^+$ fragments. In contrast to all other $\{[Au_9E_4(dppx)_3]\}_2^{2+}$ cations published so far, the two subunits in **1** are not interconnected in a catenane-like way. For comparison Figure 1d shows an analogous drawing of the core of $[Au_9Se_4(dppe)_3]_2^{2+}$ [dppe = bis(diphenylphosphanyl)ethane][2a] demonstrating the catenation of the two $[Au_9Se_4(dppe)_3]^+$ cations. Because of this significant difference it was particularly intriguing to employ electrospray mass spectrometry to gain insight into the relative stability of this dication. More specifically, we wondered whether this cluster dication can be observed both in solution and in the gas phase, what the possible fragmentation pathways are {e.g. scission into two singly charged $[Au_9Se_4(dppthph)_3]^+$ ions driven by Coulomb repulsion?} and how they compare to the related cluster $[Au_{18}Se_8(dppe)_6]^{2+}$ in which the two catenated Au_9Se_4 subunits are further clamped together by the bidentate ligands.[2a]

Figure 2 displays a positive-ion FT-ICR mass spectrum obtained upon electrospraying a solution of **1**: The virtually only ion signal obtained is found at $m/z \approx 3446.1$. On the basis of the exact mass and the isotopomer distribution (see inset in Figure 2) it can be clearly identified as the doubly charged species $[Au_{18}Se_8(dppthph)_6]^{2+}$. The stability of this

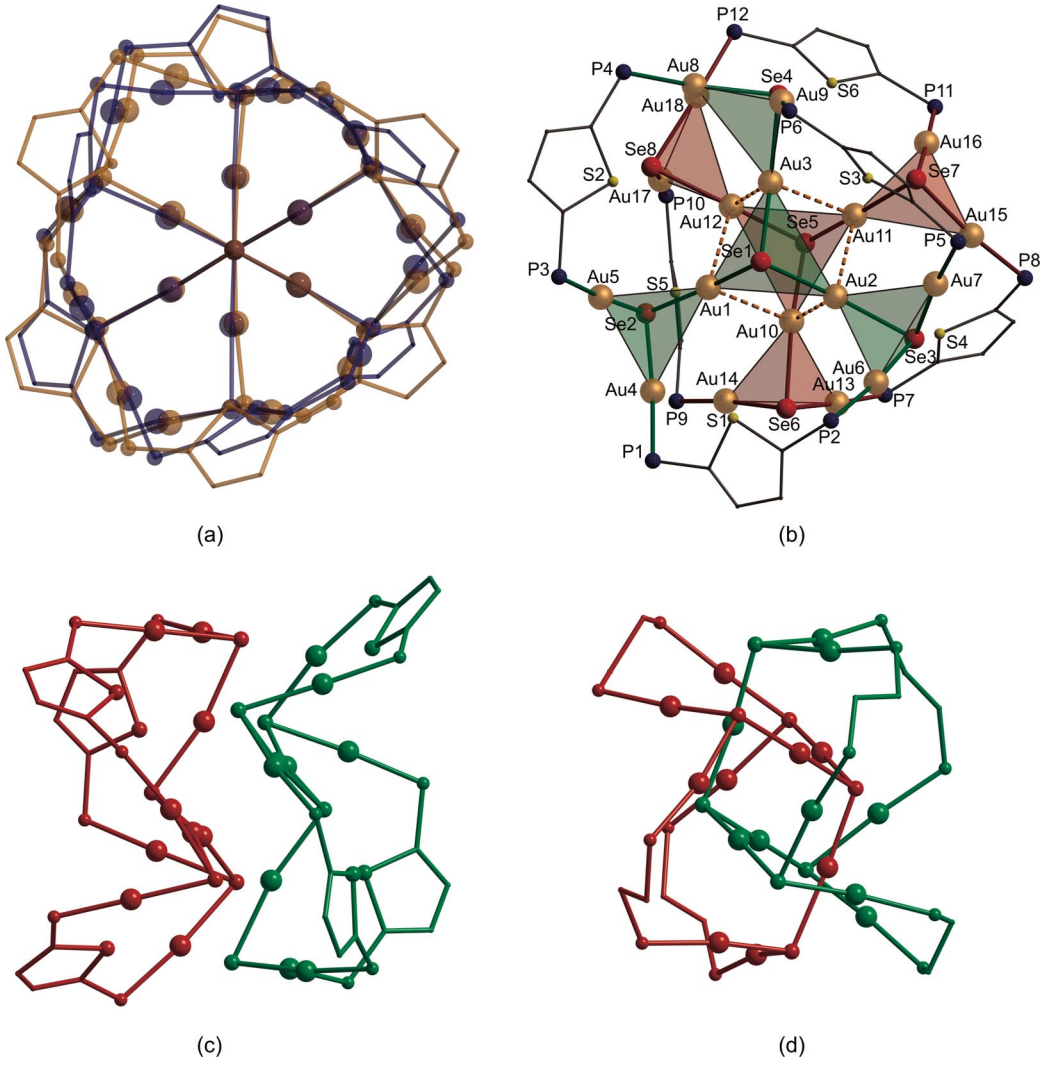

Figure 1. (a): Superposition of the cluster cores of the $[Au_{18}Se_8(dppthph)_6]^{2+}$ cations in **1a** (blue) and **1b** (orange); (b) molecular structure of the cation in **1a** (Au: gold, Se: red, P: blue, S: yellow, C: gray); (c) view of the cation in **1a** [rotated by 90° compared to Figure 1(a)] demonstrating the arrangement of the two $[Au_9Se_4(dppthph)_3]^+$ subunits (red and green); (d) view of the cation $[Au_{18}Se_8(dppe)_6]^{2+}$[2a] showing the catenane-like connection of the subunits (red and green). Selected bond lengths [pm] in the cations of **1a/1b**: Au1–Au10 299.4(1)/300.0(2), Au1–Au12 300.6(1)/299.8(2), Au2–Au10 296.8(1)/299.1(2), Au2–Au11 294.5(1)/294.9(2), Au3–Au11 301.1(1)/296.1(2), Au3–Au12 297.0(1)/294.5(2); Au1–Se1 241.9(2)/244.3(4), Au1–Se2 246.2(2)/249.3(4), Au2–Se1 243.3(2)/242.9(3), Au2–Se3 249.3(2)/248.6(3), Au3–Se1 242.7(2)/243.5(2), Au3–Se4 247.4(2)/243.1(4), Au4–Se2 242.3(2)/242.6(3), Au5–Se2 242.1(2)/244.1(4), Au6–Se3 242.1(2)/243.9(4), Au7–Se3 244.0(2)/243.3(4), Au8–Se4 244.4(2)/244.0(4), Au9–Se4 243.4(2)/245.1(3), Au10–Se5 243.2(2)/242.4(4), Au10–Se6 248.4(2)/248.5(4), Au11–Se5 242.7(2)/244.5(4), Au11–Se7 247.4(2)/250.6(4), Au12–Se5 242.2(2)/243.1(3), Au12–Se8 247.6(2)/248.3(3), Au13–Se6 244.0(2)/244.7(4), Au14–Se6 245.6(2)/241.6(4), Au15–Se7 243.6(2)/242.4(3), Au16–Se7 245.2(2)/244.5(4), Au17–Se8 245.3(2)/243.9(4), Au18–Se8 244.3(2)/243.5(4); average Au–P 225.8/225.4.

species was studied by means of collision-induced dissociation in the ICR cell of the FT mass spectrometer. Figure 3 shows the fragmentation mass spectra of the isolated parent ion $[Au_{18}Se_8(dppthph)_6]^{2+}$ at two different collision energies. At low collision energy – i.e. when fragmentation sets in and becomes observable – sequential loss of two dppthph ligands is observed (upper trace in Figure 3) without impairing the cluster's framework or charge. At somewhat higher collision energies (see lower trace of Figure 3) the framework of the cluster dication undergoes asymmetric scission according to Scheme 2.

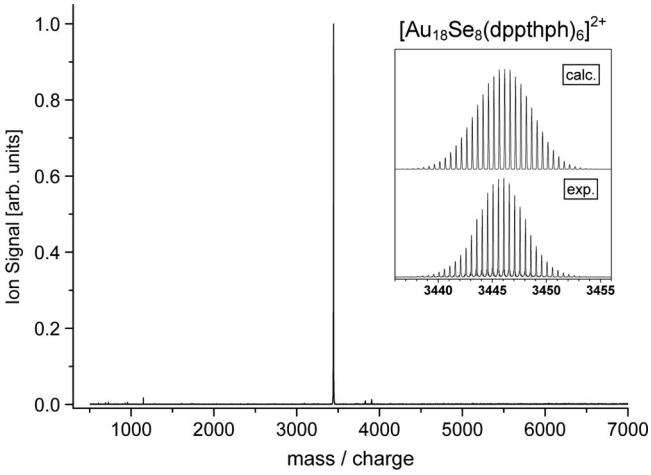

Figure 2. Positive-ion FT-ICR mass spectrum from an electrosprayed solution of **1**. The inset contrasts the experimental high-resolution signal at $m/z \approx 3446$ to the calculated isotopomer distribution for $[Au_{18}Se_8(dppthph)_6]^{2+}$.

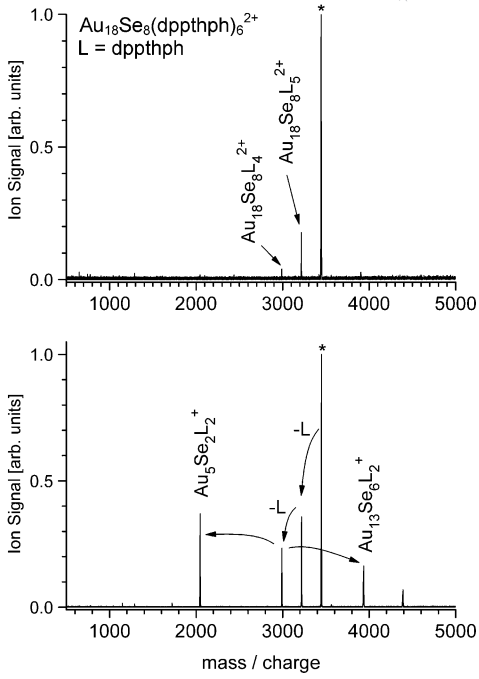

Figure 3. CID fragmentation spectra of the parent ion $[Au_{18}Se_8(dppthph)_6]^{2+}$ (marked with an asterisk) at low (upper trace) and high (lower trace) collision energies.

$$[Au_{18}Se_8(dppthph)_5]^{2+} \rightarrow [Au_{13}Se_6(dppthph)_3]^{+} + [Au_5Se_2(dppthph)_2]^{+}$$

$$[Au_{18}Se_8(dppthph)_4]^{2+} \rightarrow [Au_{13}Se_6(dppthph)_2]^{+} + [Au_5Se_2(dppthph)_2]^{+}$$

Scheme 2. Fragmentation channels observed upon collision-induced dissociation of isolated dications of **1** after loss of one and two dppthph ligands.

This is an intriguing result: Despite the two excess charges on the cluster and the known strong gold–phosphane bond,[5] loss of two neutral ligands is the primary (and therefore presumably energetically lowest-lying) fragmentation pathway before the cluster core dissociates at higher excess collision energies – presumably involving scission of the Au_6Se_2 heterocubane unit.

This observation and the rather small Au–Au average distance of 297 pm in the core immediately point towards a strong aurophilic interaction as discussed by, e.g., Schmidbaur[1a–1l] or Pyykkö[6] in detail. We investigated this question further by carrying out molecular electronic structure calculations. In a first attempt, the structures of the cluster **1b** (= dimer) and the monomer (= $[Au_9Se_4(dppthph)_3]^{+}$) were optimized by the density functional theory (DFT) level of theory, which predicted the cluster to be energetically unstable, with the monomers favored by 21 kJ/mol.[7] It is well known, however, that DFT is not able to describe van der Waals type interactions (to which aurophilic interactions belong) properly, and thus, DFT cannot be regarded reliable in this case.

Therefore, we investigated the bonding conditions adopting the SCS-MP2 (spin-component scaled Møller–Plesset perturbation theory of second order) level of theory as proposed by Grimme,[8] which gives more reliable results for gold cluster compounds than ordinary MP2,[9] which is known to overbind van der Waals complexes in general. In this part of the study we considered only the heterocubane core $(Au_3Se)_2^{2+}$ as illustrated in Figure 4, and computed the potential energy surface for pulling apart the two Au_3Se^{+} subunits, which is also shown in Figure 4. Au–Se bond lengths and bonding angles were kept fixed to match the experimental ones.[10] With this simple model, we obtained a quite typical curve for the dissociation of multiply charged ions, revealing a Coulomb barrier height of 122 kJ/mol for symmetric dissociation with respect to the cluster. The minimum energy distance between the Se atoms is located at 476 pm and matches the experimentally observed result (crystal structure: **1a**: 478 pm, **1b**: 492 pm). The transition-state area is found to be around 680 pm. Moreover, the SCS-MP2 calculations support the finding of the DFT calculations that the dimer is only metastable with respect to the monomers, namely 102 kJ/mol, i.e. even more than predicted by DFT (albeit for a larger dication). To conclude, the observed stability of the cluster core is due to aurophilic interactions which are accompanied by a relatively high Coulomb barrier.

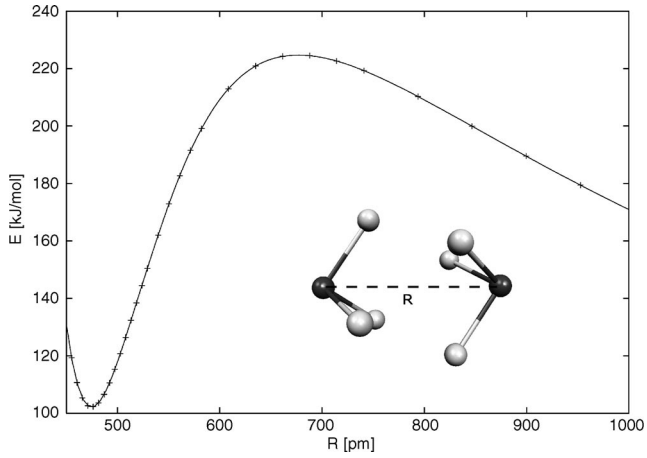

Figure 4. Potential energy surface for the symmetric dissociation and picture of the $(Au_3Se)_2^{2+}$ model complex at the SCS-MP2/QZVPP level of theory. The energy is relative to the completely separated monomers.

In accordance with the structural similarity of the two crystal modifications of **1**, we measured virtually identical FT-Raman spectra of **1a** and **1b**, particularly in the frequency range of $\geq 500\ cm^{-1}$, which is likely dominated by vibrational modes of the dppthph ligands. On the other hand, photoluminescence (PL) spectroscopy evidenced notable differences in the electronic structure and relaxation dynamics of **1a** and **1b**. Both crystals exhibited red emission under illumination in the UV/Vis spectral range, however, with distinct PL excitation (PLE) and emission spectra as shown in Figure 5. The emission maxima of **1a** and **1b** underwent uneven blueshifts from 647 and 660 nm, respectively, to 630 and 625 nm, respectively, by decreasing the temperature from 293 to 15 K (Figure 5). The PLE spectrum of **1b** is weakly structured as compared to **1a** and shows an additional shoulder at ca. 550–580 nm. The differences in the PLE spectra are consistent with the distinctly perceived colors of **1a** and **1b** (see above). PL quantum efficiency, ϕ_{PL}, of **1a** and **1b** at ambient temperature was only $(3–4)\times10^{-2}$ and $(4–6)\times10^{-3}$, respectively, but it significantly increased by decreasing the temperature (Figure 5). The changes in ϕ_{PL} roughly correlate with the timescale of the PL decay (well fitted with biexponential curves). The latter occurred within tens (**1b**) and hundreds (**1a**) of nanoseconds at ambient temperature and slowed down to several microseconds at 15 K. The above deviations in the PL properties may be tentatively attributed to the different orientation of the ligands and "packing" of the cluster units in **1a** and **1b** and, correspondingly, to differences in the vibronic properties between them. In this context, the crystal modifications of **1** appear to be an interesting object for further comparative experimental and theoretical studies.

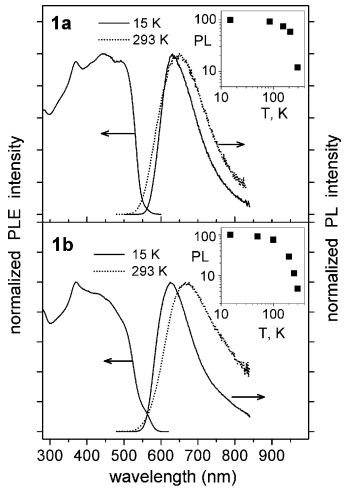

Figure 5. Normalized photoluminescence excitation (PLE) and emission (PL) spectra of crystals of **1a** (top) and **1b** (bottom) in nujol mull. The emission and excitation wavelengths for the PLE and PL spectra are 650 and 400 nm, respectively. The inserts show the temperature dependence of the integrated PL intensities.

Conclusions

This report focuses on the aurophilic interactions in the dication $[Au_{18}Se_8(dppthph)_6]^{2+}$. In the solid state the compound $[Au_{18}Se_8(dppthph)_6]Cl_2$ crystallizes in two modifications (**1a** and **1b**) in which the cations have nearly identical cores but different orientations of the thiophene and phenyl groups in the ligand shell. This results in differences in the solid-state PL and PLE spectra of the two modifications. The dication in **1** consists of two $[Au_9Se_4(dppthph)_3]^+$ units interconnected by six aurophilic Au···Au contacts (av. distance 289 pm). These are strong enough to stabilize the dimeric cation even in the gas phase which was demonstrated by ESI MS. By SCS-MP2 calculations the height of Coulomb barrier for symmetric dissociation can be approximated as 122 kJ/mol.

Experimental Section

General: All experiments regarding the synthesis were carried out under dry nitrogen. CH_2Cl_2 was dried with P_2O_5 and *n*-pentane with $LiAlH_4$. $Se(SiMe_3)_2$ was synthesized from Me_3SiCl and Na_2Se according to a published method.[11] [Au(tht)Cl] (tht = tetrahydrothphhene) was prepared according to standard procedures.[12]

1: To a solution of [Au(tht)Cl] (52 mg, 0.162 mmol) in CH_2Cl_2 (10 mL), dppthph (37 mg, 0.081 mmol) was added to give a colorless solution. After 30 min of stirring, $Se(SiMe_3)_2$ (0.020 mL, 0.081 mmol) was added to the former solution to give a yellow solution. This solution was layered with *n*-pentane, and a few days later yellow crystals of **1a** and orange crystals of **1b** had formed. For the spectroscopic measurements the crystals were separated manually.

X-ray Structure Determination: Data were collected with a STOE IPDS II diffractometer using Mo-K_α radiation (λ = 0.71073 Å). Structure solution and refinement against F^2 were carried out using SHELXS and SHELXL software.[13] Further details are given in ref.[3]

Mass Spectrometry: Mass spectra were taken with a Fourier transform ion cyclotron resonance (FT-ICR) mass spectrometer (Bruker Daltonics, APEX II) equipped with a 7 T magnet and an electrospray ionization source (Analytica of Branford) with a set of home-

built rf ion optics for improved sensitivity. Solutions from hand-picked crystals containing **1a** in dichloromethane (CH_2Cl_2) were prepared and sprayed using nitrogen as nebulizing gas at a flow rate of 300 μL/h. The desolvation capillary was typically heated to about 80 °C. Collision-induced dissociation was performed employing resonant dipolar rf excitation of the parent ion to variable kinetic energies in the ICR cell and using argon as collision gas at a typical pressure of 3×10^{-7} mbar.

Photoluminescence Spectroscopy: Photoluminescence spectra of nujol mulls of crystals of **1a** and **1b** were measured with a Spex Fluorolog-3 spectrometer equipped with a closed-cycle optical cryostat (Leybold) operating at 15–293 K. Emission spectra were corrected for the wavelength-dependent response of the spectrometer.[2b] An integrating sphere was applied to estimate the PL quantum efficiency of **1a** and **1b** at ambient temperature according to a procedure described in ref.[2b] Emission decay traces were recorded using an N_2 laser (337 nm, ≤ 4 ns) for a pulse excitation.

Calculations: All calculations were carried out with the TURBOMOLE program suite.[14] Geometry optimizations[15] of the cluster and the monomer were performed by adopting the TPSS[16] density functional in combination with the def2-TZVP basis sets from the TURBOMOLE library and the RI-J approximation.[17] The reported potential energy surface was scanned at the SCS-MP2 level of theory[18] with the def2-QZVPP basis sets.[19] Basis set incompleteness problems were considered by adopting counterpoise corrections (to avoid basis-set superposition errors) and basis-set extrapolation on selected points of the potential surface, but it was found that these effects approximately cancel each other for the above-mentioned basis set. A relativistic small core pseudo potential for gold was used throughout.[20]

Acknowledgments

This work was supported by the Deutsche Forschungsgemeinschaft (Center for Functional Nanostructures), the Deutsch-Israelisches Programm (DIP), and the Fonds der Chemischen Industrie.

[1] a) H. Schmidbaur, G. Weidenhiller, O. Steigelmann, *Angew. Chem.* **1991**, *103*, 442–444; *Angew. Chem. Int. Ed. Engl.* **1991**, *30*, 433–435; b) H. Schmidbaur, O. Steigelmann, *Z. Naturforsch* **1992**, *47b*, 1721–1724; c) E. Zeller, H. Beruda, H. Schmidbaur, *Inorg. Chem.* **1993**, *32*, 3203–3204; d) N. Dufour, A. Schier, H. Schmidbaur, *Organometallics* **1993**, *12*, 2408–2410; e) E. Zeller, H. Schmidbaur, *J. Chem. Soc. Chem. Commun.* **1993**, 69–70; f) A. Blumenthal, H. Beruda, H. Schmidbaur, *J. Chem. Soc. Chem. Commun.* **1993**, 1005–1006; g) O. Steigelmann, P. Bissinger, H. Schmidbaur, *Z. Naturforsch.* **1993**, *48b*, 72–78; h) G. M. T. Cheetham, M. M. Harding, J. L. Haggitt, D. M. P. Mingos, H. R. Powell, *J. Chem. Soc. Chem. Commun.* **1993**, 1000–1001; i) E. Zeller, H. Beruda, H. Schmidbaur, *Chem. Ber.* **1993**, *126*, 2033–2036; j) H. Beruda, E. Zeller, H. Schmidbaur, *Chem. Ber.* **1993**, *126*, 2037–2040; k) H. Schmidbaur, S. Hofreiter, M. Paul, *Nature* **1995**, *377*, 503–504; l) R. E. Bachman, H. Schmidbaur, *Inorg. Chem.* **1996**, *35*, 1399–1401; m) R. C. B. Copley, D. M. P. Mingos, *J. Chem. Soc. Dalton Trans.* **1996**, 479–489; n) J. Phete, C. Maichle-Mössmer, J. Strähle, *Z. Anorg. Allg. Chem.* **1998**, *624*, 1207–1210; o) J. Phete, J. Strähle, *Z. Naturforsch.* **1999**, *54b*, 381–384.

[2] a) D. Fenske, T. Langetepe, M. M. Kappes, O. Hampe, P. Weis, *Angew. Chem.* **2000**, *112*, 1925–1928; *Angew. Chem. Int. Ed.* **2000**, *39*, 1857–1860; b) S. Lebedkin, T. Langetepe, P. Sevillano, D. Fenske, M. M. Kappes, *J. Phys. Chem. B* **2002**, *106*, 9019–9026; c) P. Sevillano, T. Langetepe, D. Fenske, *Z. Anorg. Allg. Chem.* **2003**, *629*, 207–214; d) J. Olkowska-Oetzel, P. Sevillano, A. Eichhöfer, D. Fenske, *Eur. J. Inorg. Chem.* **2004**, 1100–1106; e) P. Sevillano, O. Fuhr, M. Kattannek, P. Nava, O. Hampe, S. Lebedkin, R. Ahlrichs, D. Fenske, M. M. Kappes, *Angew. Chem.* **2006**, *118*, 3785–3791; *Angew. Chem. Int. Ed.* **2006**, *45*, 3702–3708; f) P. Sevillano, O. Fuhr, E. Matern, D. Fenske, *Z. Anorg. Allg. Chem.* **2006**, *632*, 735–738; g) P. Sevillano, O. Fuhr, O. Hampe, S. Lebedkin, E. Matern, D. Fenske, M. M. Kappes, *Inorg. Chem.* **2007**, *46*, 7294–7298.

[3] Crystallographic data: **1a**: $[Au_{18}Se_8(dppthph)_6]Cl_2 \cdot 9CH_2Cl_2$: $C_{177}H_{150}Au_{18}Cl_{20}P_{12}S_6Se_8$; triclinic, space group $P\bar{1}$, $Z = 2$; $a = 1819.2(4)$, $b = 2402.5(5)$, $c = 2499.9(5)$ pm, $\alpha = 95.37(3)$, $\beta = 91.07(3)$, $\gamma = 103.53(3)°$; $V = 10567(4) \times 10^6$ pm^3; $T = 180(2)$ K; $\rho_{calcd.} = 2.429$ g cm^{-3}, 57341 data measured of which 34770 were unique ($R_{int} = 0.0784$); 2026 parameters; $GoF = 1.017$, $wR_2 = 0.206$ (all data); $R_1 = 0.078$ [$I > 2\sigma(I)$]; largest diff. peak/hole: 4.63/–5.96 eA^{-3} [the relatively high remaining electron density is located close to Au2 (95.3 pm)]; **1b**: $[Au_{18}Se_8(dppthph)_6]Cl_2 \cdot 9CH_2Cl_2$: $C_{177}H_{150}Au_{18}Cl_{20}P_{12}S_6Se_8$; orthorhombic, $P2_12_12_1$, $Z = 4$; $a = 2674.4(5)$, $b = 2861.1(6)$, $c = 3005.0(6)$ pm; $V = 22993(8) \times 10^6$ pm^3; $T = 180(2)$ K; $\rho_{calcd.} = 2.232$ g cm^{-3}, 41520 data measured of which 29252 were unique ($R_{int} = 0.0835$); 1259 parameters, 24 restrains; $GoF = 1.015$, $wR_2 = 0.195$ (all data); $R_1 = 0.071$ [$I > 2\sigma(I)$]; Flack parameter: 0.03; largest diff. peak/hole: 2.62/–2.60 eA^{-3}. CCDC-655627 (**1a**) and -655628 (**1b**) contain the supplementary crystallographic data for this paper. These data can be obtained free of charge from The Cambridge Crystallographic Data Centre via www.ccdc.cam.ac.uk/data_request/cif.

[4] T. Langetepe, Ph. D. Thesis, University of Karlsruhe (TH), **2001**.

[5] D. Schröder, H. Schwarz, J. Hrušák, P. Pyykkö, *Inorg. Chem.* **1998**, *37*, 624.

[6] P. Pyykkö, *Angew. Chem.* **2004**, *116*, 4512–4557; *Angew. Chem. Int. Ed.* **2004**, *43*, 4412–4456.

[7] Selected bond lengths of the optimized structure: Au···Au (within the heterocubane unit) 303.0 pm, Au–Se (within the heterocubane unit) 246.6 pm, Au–Se (from the heterocubane unit to Se outside of it) 251.3 pm; for experimental values see Figure 1.

[8] S. Grimme, *J. Chem. Phys.* **2003**, *118*, 9095–9102.

[9] S. Grimme, private communication, **2006**.

[10] Full relaxation of the core causes a collapse of the structure with the gold atoms approaching each other and the selenium atoms pushed apart. Obviously, this movement is hindered by the bulky side groups attached to the gold atoms in the full cluster.

[11] M. Schmidt, H. Ruf, *Z. Anorg. Allg. Chem.* **1963**, *321*, 270–273.

[12] R. Uson, A. Laguna, M. Laguna, *Inorg. Synth.* **1989**, *26*, 85–91.

[13] G. M. Sheldrick, *SHELXTL-97, Program for the Refinement of Crystal Structures*, University of Göttingen, **1997**.

[14] R. Ahlrichs, M. Baer, M. Haeser, H. Horn, C. Koelmel, *Chem. Phys. Lett.* **1989**, *162*, 165–169.

[15] M. v. Arnim, R. Ahlrichs, *J. Comput. Chem.* **1999**, *111*, 9183–9190.

[16] J. Tao, J. Perdew, V. N. Staroverov, G. E. Scuseria, *Phys. Rev. Lett.* **2003**, *91*, 146401.

[17] a) O. Treutler, R. Ahlrichs, *J. Chem. Phys.* **1995**, *102*, 346–354; b) F. Weigend, *Phys. Chem. Chem. Phys.* **2006**, *8*, 1057–1065; c) M. Sierka, A. Hogekamp, R. Ahlrichs, *J. Chem. Phys.* **2003**, *118*, 9136–9148.

[18] F. Weigend, M. Häser, *Theo. Chem. Acc.* **1997**, *97*, 331–340.

[19] F. Weigend, R. Ahlrichs, *Phys. Chem. Chem. Phys.* **2005**, *7*, 3297–3305.

[20] D. Andrae, U. Haeussermann, M. Dolg, H. Stoll, H. Preuss, *Theor. Chim. Acta* **1990**, *77*, 123–141.

Received: August 21, 2007
Published Online: October 11, 2007

